RAA 2016 Vol. **16** No. **7**, 103 (14pp) doi: 10.1088/1674–4527/16/7/103
http://www.raa-journal.org *http://iopscience.iop.org/raa*

***R**esearch in*
***A**stronomy and*
***A**strophysics*

Comparison between TeV and non-TeV BL Lac Objects

Chao Lin and Jun-Hui Fan

Center for Astrophysics, Guangzhou University, Guangzhou 510006, China; *fjh@gzhu.edu.cn*
Astronomy Science and Technology Research Laboratory of Department of Education of Guangdong Province, Guangzhou 510006, China

Received 2015 October 1; accepted 2016 March 21

Abstract BL Lacertae objects (BL Lacs) are the dominant population of TeV emitting blazars. In this work, we investigate whether there are any special observational properties associated with TeV sources. To do so, we will compare the observational properties of TeV detected BL Lacs (TeV BLs) with non-TeV detected BL Lac objects (non-TeV BLs). From the 3rd *Fermi*/LAT source catalog (3FGL), we can obtain 662 BL Lacs, out of which 47 are TeV BLs and 615 are non-TeV BLs. Their multi-wavelength flux densities ($F_{\rm R}$, $F_{\rm O}$, $F_{\rm X}$ and F_γ), photon spectral indexes ($\alpha_{\rm X}^{\rm ph}$ and $\alpha_\gamma^{\rm ph}$), and effective spectral indexes ($\alpha_{\rm RO}$ and $\alpha_{\rm OX}$) are compiled from the available literature. Then the luminosities ($\log \nu L_{\rm R}$, $\log \nu L_{\rm O}$, $\log \nu L_{\rm X}$, $\log \nu L_\gamma$) are calculated. From comparisons, we find that TeV BLs are different from low synchrotron peaked BLs and intermediate synchrotron peaked BLs, but TeV BLs show similar properties to high synchrotron peaked (HSP) BLs. Therefore, we concentrated on a comparison between TeV HSP BLs and non-TeV HSP BLs. Analysis results suggest that TeV HSP BLs and non-TeV HSP BLs exhibit some differences in their $\alpha_{\rm RO}$ and $\alpha_\gamma^{\rm ph}$, but their other properties are quite similar.

Key words: galaxies: active — BL Lacertae objects: general — gamma rays: galaxies

1 INTRODUCTION

Blazars are a subclass of active galactic nuclei (AGNs). They have high and variable polarization, large and rapid variation, superluminal motions, highly energetic GeV (even TeV) γ-ray emissions, etc (Wills et al. 1992; Zhang & Fan 2008; Gupta et al. 2008; Romero et al. 2002; Abdo et al. 2010b; Bastieri et al. 2011; Fan et al. 2013a, 2014; Ackermann et al. 2015). Blazars can be divided into two subclasses, namely, flat spectrum radio quasars (FSRQs) and BL Lacertae objects (BL Lacs). BL Lacs show no (or very weak) emission line features but FSRQs display strong emission lines. However, BL Lacs and FSRQs show quite similar continuum emission properties. BL Lacs can be divided into radio selected BL Lacertae objects and X-ray selected BL Lacertae objects from surveys or low synchrotron peaked (LSP, $\nu_{\rm peak}^{\rm s} < 10^{14}$ Hz), intermediate synchrotron peaked (ISP, 10^{14} Hz $< \nu_{\rm peak}^{\rm s} < 10^{15}$ Hz), and high synchrotron peaked (HSP, $\nu_{\rm peak}^{\rm s} > 10^{15}$ Hz) BL Lacs from the description by Abdo et al. (2010c) (also see Fan et al. 2014, 2016, submitted; Ackermann et al. 2015). In 2015, we set different limits: LSP ($\nu_{\rm peak}^{\rm s} < 10^{14}$ Hz), ISP (10^{14} Hz $< \nu_{\rm peak}^{\rm s} < 10^{16}$ Hz), and HSP ($\nu_{\rm peak}^{\rm s} > 10^{16}$ Hz, Fan et al. 2015). Thanks to the work of the *Energetic Gamma Ray Experiment Telescope* (*EGRET*), γ-ray astronomy has made great strides forward. As the second generation of γ-ray detectors, the *Fermi*/LAT satellite was launched on 2008 June 11 and has detected many blazars at γ-ray energies (Abdo et al. 2010b; Nolan et al. 2012; Lott et al. 2015; Acero et al. 2015; Ackermann et al. 2015). The 3rd *Fermi* Large Area Telescope source catalog (3FGL) includes 3033 sources in the range 100 MeV–300 GeV. Such a large sample of sources gives us a nice opportunity to analyze the nature of γ-ray emissions from blazars.

Highly energetic emissions, as high as TeV, are also detected from some blazars, and most of them have also been detected by *Fermi*/LAT (Ackermann et al. 2015). From TeVCat[1], we found that there were 176 sources detected in the TeV energy range until March, 2016. These sources were included in TeV catalogs called the "Default Catalog" and "Newly Announced." The energy threshold for the TeVCat sources is not uniform, but the energy is typically greater than 100 GeV (Acero et al. 2015). The known extragalactic TeV sources are mainly BL Lacs, but we want to investigate what kind of BL Lacs are TeV emitters, so we compared the known TeV BLs with BL Lacs detected in *Fermi*/LAT.

In this work, we compile BL Lacs from 3FGL and then compare observational properties of TeV BL Lacs and non-TeV BL Lacs, and try to see whether there is any difference between them. In Section 2, we give a sample, in Section 3, we show some results and in Section 4, we provide some discussion and conclusions.

[1] *http://tevcat.uchicago.edu/*

2 SAMPLE

Based on the 3FGL (Acero et al. 2015), the third catalog of AGNs detected by the *Fermi*-LAT (3LAC) is presented (Ackermann et al. 2015). 3LAC not only compiles the γ-ray data of AGNs detected by *Fermi*–LAT during the first four years, but also collects the fluxes at different bands (radio, optical and X-ray) and some other data. From 3LAC, we can obtain 662 *Fermi* BL Lacs, their redshift, spectral energy distribution (SED) classification (based on the synchrotron peak frequency), radio flux ($F_{\rm R}$) at 1.4 GHz, SDSS V band magnitude (m_V), X-ray flux ($F_{\rm X}$) at 0.1–2.4 keV, γ-ray flux (F_γ) at 1–100 GeV, and γ-ray power-law photon index ($\alpha_\gamma^{\rm ph}$). The effective spectral indexes ($\alpha_{\rm RO}$ and $\alpha_{\rm OX}$) for BL Lacs are from the website version[2] of 3LAC. For some sources in 3LAC, if there were not data available in the 3LAC website, we looked for them in the NASA/IPAC Extragalactic Database (NED)[3]. For optical data, if the V band magnitude was not available in 3LAC and NED, we used the R band magnitude from NED and $\alpha_O = 1.0$ to estimate it. For the 662 *Fermi* BL Lacs, 332 BL Lacs had available SDSS V band magnitude from 3LAC, and 24/60 BL Lacs had available V/R band magnitude from NED. For X-ray data, if X-ray flux was not available in 3LAC, we compiled the data from the BZCAT version 5.0.0 [4] (Massaro et al. 2015) and NED (April, 2015), and the corresponding X-ray photon indexes ($\alpha_{\rm X}^{\rm ph}$) were from the corresponding references.

Combining the 662 *Fermi* BL Lacs and the TeV sources listed in table 13 of Ackermann et al. (2015), we could obtain a sample of 47 BL Lacs with both TeV and GeV emissions, which are listed in Table 1. Since the TeV sample of Ackermann et al. (2015) was from TeVCat, the TeV sources in this work are the ones detected in the range $E \geq 100$ GeV. For the remaining 615 *Fermi* BL Lacs that have no TeV emissions, we did not list their data in the present work.

3 RESULTS

In this work, luminosity is calculated using $\nu L_\nu = 4\pi d_{\rm L}^2 \nu F_\nu$, where $d_{\rm L}$ is the luminosity distance. The Cosmology Calculator I [5] from NED is used to compute the luminosity distance (Wright 2006). Here we adopt $H_0 = 73$ km s^{-1} Mpc^{-1}, $\Omega_{\rm M} = 0.27$ and $\Omega_{\rm vac} = 0.73$. All the fluxes are K-corrected. The flux in the source rest frame is $F_\nu^{\rm res} = F_\nu^{\rm obs}(1+z)^{\alpha-1}$ and α ($F_\nu \propto \nu^{-\alpha}$) is the energy spectral index (Kapanadze 2013). $\alpha_{\rm R}$ = 0.0 and $\alpha_{\rm O}$ = 1.0 are adopted for radio and optical bands respectively, $\alpha_{\rm X} = \alpha_{\rm X}^{\rm ph} - 1$ and $\alpha_\gamma = \alpha_\gamma^{\rm ph} - 1$. Most of the X-ray spectral indexes are given for 0.1–2.4 keV. If there is no spectral index information in the 0.1–2.4 keV band, but there is a spectral index in the hard X-ray band, then we use the spectral index in the hard X-ray band instead. If redshift and X-ray photon index are unknown, then averaged values $\langle z \rangle$ = 0.463 and $\langle \alpha_{\rm X}^{\rm ph} \rangle = 2.35$ are adopted. For optical V band luminosity calculation, V band magnitude (m_V) is transferred into flux density (F_V) using $m_V = 16.40 - 2.5 \log F_V$, where F_V is the flux density in units of mJy (Kapanadze 2013). All the V band magnitudes are corrected by Galactic Extinction from NED.

For the 662 BL Lacs in 3LAC, there are 286 HSP, 185 ISP, 168 LSP and 23 with unknown SED type. Out of the 662 BL Lacs, there are 47 TeV BL Lacs (including 40 HSP, 3 ISP, 2 LSP and 2 with unknown SED type). For the TeV BLs and non-TeV BLs, we made some comparisons for z, $\alpha_{\rm X}^{\rm ph}$, $\alpha_\gamma^{\rm ph}$, $\log \nu L_{\rm R}$, $\log \nu L_{\rm O}$, $\log \nu L_{\rm X}$, $\log \nu L_\gamma$, $\alpha_{\rm RO}$ and $\alpha_{\rm OX}$ as follows.

3.1 Averaged Values

For the whole sample, the redshift is in a range of $0.002 \leq z \leq 2.471$; X-ray and γ-ray photon spectral indexes are $1.03 \leq \alpha_{\rm X}^{\rm ph} \leq 4.28$ and $1.26 \leq \alpha_\gamma^{\rm ph} \leq 2.81$ respectively; radio, optical, X-ray and γ-ray luminosities are in the ranges: 36.30 erg s^{-1} $\leq \log \nu L_{\rm R} \leq$ 44.10 erg s^{-1}, 40.29 erg s^{-1} $\leq \log \nu L_{\rm O} \leq$ 47.03 erg s^{-1}, 39.45 erg s^{-1} $\leq \log \nu L_{\rm X} \leq$ 46.45 erg s^{-1}, and 39.24 erg s^{-1} $\leq \log \nu L_\gamma \leq$ 47.33 erg s^{-1} respectively; effective spectral indexes satisfy $-0.13 \leq \alpha_{\rm RO} \leq 0.96$ and $0.43 \leq \alpha_{\rm OX} \leq 2.52$. The corresponding averaged values are listed in Table 2, and the corresponding Kolmogorov-Smirnov (K-S) test results are listed in Table 3, in which, Col. (1) gives two tested samples, Col. (2) tested parameter, Col. (3) number of two samples, Col. (4) average value and standard deviation, Col. (5) K-S statistic $d_{\rm max}$, and Col. (6) two-tailed significance probability p. The sample with "$*$" is only for sources with available redshift and p is the probability for the two distributions to come from the same distribution. The corresponding histograms and cumulative probabilities are shown in Figures 1–9.

From Tables 2 and 3, and the corresponding Figures 1–9, we can see that, for redshift, TeV BLs are clearly different from non-TeV BLs, HSP BLs and ISP+LSP BLs with probabilities for the corresponding two groups to come from the same distribution being $p < 10^{-5}$, suggesting that the redshift of TeV BLs is lower than those of the other groups. For the X-ray photon index, TeV BLs are not different from non-TeV BLs, HSP BLs or ISP+LSP BLs. For the γ-ray photon index and radio luminosity, TeV BLs are clearly different from non-TeV BLs and ISP+LSP BLs, but not different from HSP BLs. For optical luminosity, TeV BLs are marginally different from non-TeV and ISP+LSP BLs, but not different from HSP BLs. For X-ray luminosity and the effective optical-X-ray spectral index, there is not much difference between TeV and non-TeV BLs or HSP BLs, but TeV BLs are different from ISP+LSP BLs. For γ-ray luminosity and the effective radio-optical spectral index, TeV BLs are clearly different from non-TeV BLs

[2] *http://www.asdc.asi.it/fermi3lac/*

[3] *http://ned.ipac.caltech.edu/*

[4] *http://www.asdc.asi.it/bzcat*

[5] *http://www.astro.ucla.edu/∼wright/CosmoCalc.html*

Table 1 TeV Sample of the BL Lacs

3FGL Name	z	SED	$\log \nu_{\rm p}^{\rm s}$	$\alpha_\gamma^{\rm ph}$	$F_{\rm X}$	Ref$_1$	$\alpha_{\rm RO}$	$\alpha_{\rm OX}$	TeV	$\alpha_{\rm X}^{\rm ph}$	Ref$_2$	$\log \nu L_{\rm R}$	$\log \nu L_{\rm O}$	$\log \nu L_{\rm X}$	$\log \nu L_\gamma$	Other name
(1)	(2)	(3)	(4)	(5)	(6)	(7)	(8)	(9)	(10)	(11)	(12)	(13)	(14)	(15)	(16)	(17)
3FGL J0013.9–1853	0.094	HSP	16.76	1.94	12.60	LAC	–0.01	1.58	T			39.89		43.79	42.89	RBS 0030
3FGL J0033.6–1921	0.610	HSP	16.13	1.71	14.90	LAC	0.20	1.03	T			41.38		45.78	45.71	KUV 00311–1938
3FGL J0035.9+5949		HSP	17.12	1.90	31.80	LAC			T	1.42	G02	42.03	45.84	45.90	45.48	1ES 0033+595
3FGL J0136.5+3905		HSP	16.20	1.70	23.30	LAC	0.29	1.04	T	2.16	B97b	41.64		45.71	45.67	B3 0133+388
3FGL J0152.6+0148	0.080	HSP	15.46	1.89	6.07	LAC	0.20	1.45	T	2.48	B97b	40.07	44.78	43.27	43.24	PMN J0152+0146
3FGL J0222.6+4301	0.444	HSP	15.09	1.94	6.39	LAC	0.40	1.49	T	2.20	G02	43.18	46.23	45.10	46.31	3C 66A
3FGL J0232.8+2016	0.139	HSP	15.48	2.03	15.70	LAC	0.23	1.22	T	1.99	D05	40.69	45.00	44.37	43.53	1ES 0229+200
3FGL J0303.4–2407	0.260	HSP	15.43	1.92	10.20	LAC	0.45	1.20	T	2.68	F12	42.18		44.57	45.24	PKS 0301–243
3FGL J0319.8+1847	0.190	HSP	16.99	1.57	27.00	LAC	0.30	0.80	T	1.50	G02	40.41	44.59	44.98	43.85	RBS 0413
3FGL J0349.2–1158	0.185	HSP	18.29	1.73	30.90	LAC	0.23	0.83	T	2.03	D05	40.42	44.54	44.93	43.61	1ES 0347–121
3FGL J0416.8+0104	0.287	HSP	16.64	1.75	73.20	LAC	0.33	0.82	T	2.80	R00	41.50	45.27	45.48	44.33	1ES 0414+009
3FGL J0449.4–4350	0.205	HSP	15.67	1.85	14.30	LAC	0.38	1.19	T			41.70		44.60	45.24	PKS 0447-439
3FGL J0508.0+6736	0.340	HSP	17.75	1.52	35.90	LAC	0.30	0.82	T	2.31	G02	41.00		45.53	44.93	1ES 0502+675
3FGL J0521.7+2113	0.108	ISP	14.38	1.92	6.02	LAC			T	1.21	B97b	41.27		43.82	44.54	TXS 0518+211
3FGL J0550.6–3217	0.069			1.61	51.20	LAC	0.11	1.46	T	2.28	D05	40.68	44.16	44.14	42.58	PKS 0548–322
3FGL J0648.8+1516	0.179	HSP	15.92	1.83	38.10	LAC			T			40.81		44.89	44.25	RX J0648.7+1516
3FGL J0650.7+2503	0.203	HSP	16.42	1.72	42.30	LAC	0.28	1.02	T	2.47	F12	41.09		45.02	44.52	1ES 0647+250
3FGL J0710.3+5908	0.125	HSP	16.99	1.66	32.50	LAC	0.19	1.14	T	2.15	F12	40.88		44.54	43.51	1H 0658+595
3FGL J0721.9+7120	0.127	LSP	13.99	2.04	4.91	LAC	0.43	1.50	T	2.10	R00	41.55	45.38	43.75	45.15	S5 0716+71
3FGL J0809.8+5218	0.138	HSP	15.86	1.88	17.80	LAC	0.33	1.21	T	3.00	R00	41.02	45.05	44.00	44.52	1ES 0806+524
3FGL J0847.1+1134	0.199	HSP	15.95	1.74	23.80	LAC	0.36	0.80	T	2.50	B97b	40.61	44.62	44.74	43.87	RX J0847.1+1133
3FGL J1010.2–3120	0.143	HSP	16.31	1.58	28.30	LAC	0.14	1.31	T			40.67		44.54	43.71	1RXS J101015.9–311909
3FGL J1015.0+4925	0.212	HSP	15.63	1.83	19.80	LAC	0.39	1.16	T	2.48	F12	41.73	45.33	44.73	45.12	1H 1013+498
3FGL J1103.5–2329	0.186	HSP	17.19	1.64	50.90	LAC	0.32	0.88	T	2.25	G02	41.11		45.09	43.68	1ES 1101–232
3FGL J1104.4+3812	0.031	HSP	17.07	1.77	678.00	LAC	0.29	0.92	T	2.82	F12	40.33	44.60	44.28	43.96	Mkn 421
3FGL J1136.6+7009	0.045	HSP	15.77	1.82	56.70	LAC	0.02	1.70	T	2.20	R00	40.28	43.94	43.83	42.94	Mkn 180
3FGL J1217.8+3007	0.130	HSP	15.26	1.97	86.40	LAC	0.42	0.94	T	2.47	B00	41.47	44.99	44.89	44.60	1ES 1215+303
3FGL J1221.3+3010	0.182	HSP	16.66	1.66	31.60	LAC	0.30	0.98	T	2.10	B00	40.86	44.99	44.91	44.58	PG 1218+304
3FGL J1221.4+2814	0.103	ISP	14.42	2.10	2.29	LAC	0.47	1.58	T	2.10	R00	41.37	44.89	43.23	44.24	W Comae
3FGL J1224.5+2436	0.218	HSP	15.39	1.89	2.75	LAC	0.29	1.27	T	2.22	B00	40.59	44.88	43.99	44.14	MS 1221.8+2452
3FGL J1427.0+2347		HSP	15.34	1.82	6.94	LAC	0.32	1.51	T	2.54	B00	42.49	46.57	45.08	46.16	PKS 1424+240
3FGL J1428.5+4240	0.129	HSP	17.28	1.57	52.50	LAC	0.28	0.87	T	1.92	F12	40.47	44.69	44.85	43.53	H 1426+428
3FGL J1442.8+1200	0.163	HSP	16.35	1.80	13.80	LAC	0.37	0.93	T	2.20	F12	40.75	44.60	44.41	43.74	1ES 1440+122
3FGL J1517.6–2422	0.048	ISP	14.19	2.11	2.92	LAC	0.20	2.18	T	2.36	F12	41.14	44.38	42.54	43.64	AP Librae
3FGL J1555.7+1111	0.360	HSP	15.47	1.68	38.60	LAC	0.31	1.30	T	2.50	R00	42.12	46.48	45.57	45.84	PG 1553+113
3FGL J1653.9+3945	0.034	HSP	16.12	1.72	65.10	LAC	0.40	1.20	T	2.36	F12	40.72	44.57	43.57	43.54	Mkn 501
3FGL J1725.0+1152	0.018	HSP	16.01	1.89	32.00	LAC	0.29	1.16	T	2.65	F12	39.05	43.62	42.56	42.57	1H 1720+117
3FGL J1728.3+5013	0.055	HSP	16.00	1.96	39.60	LAC	0.20	1.30	T	2.39	F12	40.25	43.77	43.78	43.06	I Zw 187
3FGL J1743.9+1934	0.084	HSP	15.76	1.78	11.80	LAC	0.08	1.88	T	1.98	B97b	40.81		43.78	43.18	S3 1741+19
3FGL J2000.0+6509	0.047	HSP	16.86	1.88	114.00	LAC	0.07	1.46	T	2.68	F12	40.20	45.05	43.96	43.64	1ES 1959+650
3FGL J2001.1+4352		HSP	15.21	1.97	1.00	BZC			T			41.87		44.30	45.99	MG4 J200112+4352
3FGL J2009.3–4849	0.071	HSP	16.29	1.77	80.80	LAC	0.19	1.56	T	2.05	G02	41.28	45.07	44.44	43.77	PKS 2005–489
3FGL J2158.8–3013	0.116	HSP	15.97	1.83	572.00	LAC	0.20	1.01	T	2.57	G02	41.30	45.76	45.56	45.02	PKS 2155–304
3FGL J2202.7+4217	0.069	LSP	13.61	2.25	7.42	LAC	0.43	1.70	T	2.63	G02	41.93	44.64	43.15	44.48	BL Lacertae
3FGL J2250.1+3825	0.119			1.91	7.93	LAC	0.20	1.51	T	2.51	B97b	40.65		43.75	43.77	B3 2247+381
3FGL J2347.0+5142	0.044	HSP	15.87	1.78	29.70	LAC			T	2.13	F14	40.15	43.95	43.55	43.18	1ES 2344+514
3FGL J2359.3–3038	0.165	HSP	17.52	2.02	65.00	LAC	0.35	0.65	T	1.82	F12	40.73	44.10	45.19	43.83	H 2356–309

Notes: Col. (1) gives the 3FGL name, Col. (2) redshift, Col. (3) SED classification, Col. (4) synchrotron peak frequency ($\log \nu_{\rm p}^{\rm s}$) in the unit of Hz from 3LAC, the $\log \nu_{\rm p}^{\rm s}$ is already corrected by redshift in 3LAC. Col. (5) γ-ray photon index, Cols. (6) and (7) X-ray flux in units of 10^{-12} erg cm^{-2} s^{-1} at 0.1–2.4 keV and the corresponding references, Cols. (8) and (9) effective spectral indexes ($\alpha_{\rm RO}$ and $\alpha_{\rm OX}$ respectively), Col. (10) "T" stands for TeV sources, Cols. (11) and (12) X-ray photon index and the corresponding references, Cols. (13), (14), (15) and (16) give radio, optical, X-ray at 1 keV, and γ-ray (at 2 GeV) luminosities ($\log \nu L_\nu$) in units of erg s^{-1} respectively, Col. (17) other names. Here A09: Ajello et al. (2009); B00: Brinkmann et al. (2000); B97a: Brinkmann et al. (1997a); B97b: Brinkmann et al. (1997b); BZC: Massaro et al. (2015); D05: Donato et al. (2005); F12: Fan et al. (2012); F13: Fan et al. (2013a); G09: Green et al. (2009); LAC: Ackermann et al. (2015); L96: Lamer et al. (1996); L99: Laurent-Muehleisen et al. (1999); NED: the NASA/IPAC Extragalactic Database (*http://ned.ipac.caltech.edu/*); R00: Reich et al. (2000).

and ISP+LSP BLs, but only marginally different from HSP BLs.

3.2 Correlations between γ-ray and Other Bands

Next we applied a linear regression analysis to fluxes and luminosities to investigate the correlation between γ-ray and other bands. For luminosity-luminosity correlations, we only considered the sources with available redshift, and obtained

$$\log \nu L_\gamma = (1.052 \pm 0.099) \log \nu\, L_R + (1.087 \pm 4.041)$$

for 36 TeV HSP BLs with a correlation coefficient $r = 0.877$ and a chance probability of $p = 2.31 \times 10^{-12}$, and

$$\log \nu L_\gamma = (0.981 \pm 0.047) \log \nu L_R + (3.963 \pm 1.913)$$

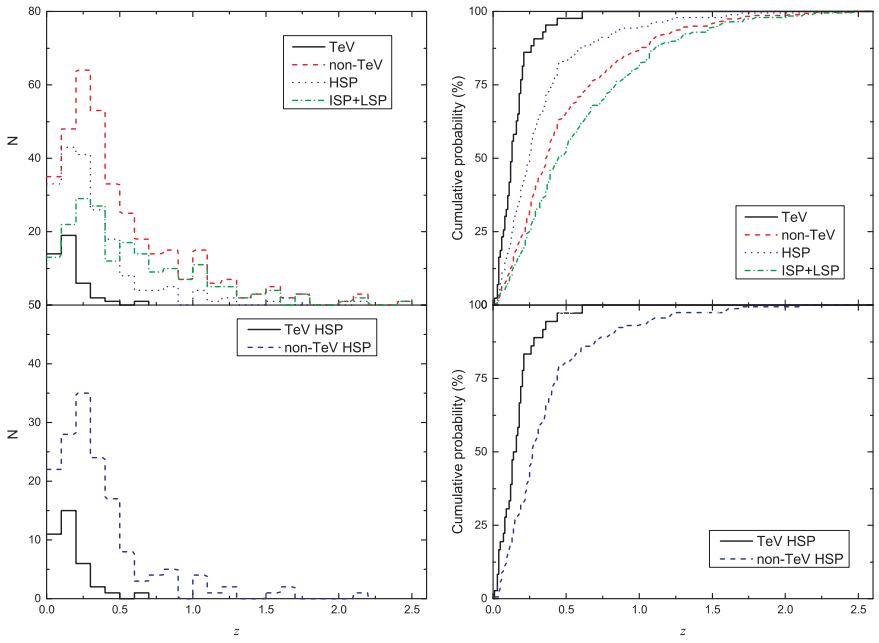

Fig. 1 The distribution of redshift (*left panels*) and the cumulative probability (*right panels*) for the whole sample (*upper panels*), and for the HSP BL Lacs (*lower panels*). In the upper panels the solid line stands for TeV sources, the dashed line for non-TeV sources, the dotted line for HSP, and the dash-dotted line for ISP+LSP. In the lower panels the solid line stands for TeV HSP BL Lacs, and the dashed line for non-TeV HSP BL Lacs.

for 157 non-TeV HSP BLs with $r = 0.861$ and $p = 2.85 \times 10^{-47}$;

$$\log \nu L_\gamma = (1.152 \pm 0.117) \log \nu L_{\rm O} - (7.611 \pm 5.242)$$

for 25 TeV HSP BLs with $r = 0.899$ and $p = 1.02 \times 10^{-9}$, and

$$\log \nu L_\gamma = (1.069 \pm 0.059) \log \nu L_{\rm O} - (3.926 \pm 2.659)$$

for 95 non-TeV HSP BLs with $r = 0.883$ and $p = 2.89 \times 10^{-32}$;

$$\log \nu L_\gamma = (0.869 \pm 0.149) \log \nu L_X + (5.375 \pm 6.633)$$

for 36 TeV HSP BLs with $r = 0.707$ and $p = 1.40 \times 10^{-6}$, and

$$\log \nu L_\gamma = (0.756 \pm 0.048) \log \nu L_X + (10.638 \pm 2.143)$$

for 151 non-TeV BLs with $r = 0.788$ and $p = 2.95 \times 10^{-33}$.

The flux densities in the unit of mJy are calculated in radio at 1.4 GHz, optical at V band, X-ray at 1 keV and γ-ray at 2 GeV. For flux-flux correlations, we have

$$\log F_\gamma = (0.752 \pm 0.126) \log F_{\rm R} - (10.794 \pm 0.280)$$

for 40 TeV HSP BLs with a correlation coefficient $r = 0.696$ and a chance probability of $p = 6.00 \times 10^{-7}$, and

$$\log F_\gamma = (0.299 \pm 0.045) \log F_{\rm R} - (10.250 \pm 0.076)$$

for 246 non-TeV HSP BLs with $r = 0.389$ and $p = 2.66 \times 10^{-10}$;

$$\log F_\gamma = (0.798 \pm 0.113) \log F_{\rm O} - (9.590 \pm 0.109)$$

for 27 TeV HSP BLs with $r = 0.769$ and $p = 2.76 \times 10^{-6}$, and

$$\log F_\gamma = (0.318 \pm 0.066) \log F_{\rm O} - (9.780 \pm 0.030)$$

for 131 non-TeV HSP BLs with $r = 0.392$ and $p = 3.73 \times 10^{-6}$;

$$\log F_\gamma = (0.073 \pm 0.184) \log F_{\rm X} - (8.982 \pm 0.480)$$

for 40 TeV HSP BLs with $r = 0.064$ and $p = 69.3\%$, and

$$\log F_\gamma = (0.054 \pm 0.039) \log F_{\rm X} - (9.585 \pm 0.136)$$

for 237 non-TeV BLs with $r = 0.089$ and $p = 17.4\%$.

$$\log F_{\rm O} = (0.744 \pm 0.147) \log F_{\rm R} - (1.076 \pm 0.340)$$

for 27 TeV HSP BLs with $r = 0.711$ and of $p = 3.19 \times 10^{-5}$, and

$$\log F_{\rm O} = (0.557 \pm 0.071) \log F_{\rm R} - (1.047 \pm 0.116)$$

for 131 non-TeV BLs with $r = 0.567$ and $p = 1.58 \times 10^{-12}$.

All the results are listed in Table 4 and shown in Figures 10–11.

4 DISCUSSION AND CONCLUSIONS

In this paper, we compiled multi-wavelength data ($\alpha_{\rm X}^{\rm ph}$, $F_{\rm R}$, $F_{\rm O}$, $F_{\rm X}$, F_γ, $\alpha_\gamma^{\rm ph}$, $\alpha_{\rm RO}$ and $\alpha_{\rm OX}$) for a sample of 662 BL Lacs from the 3LAC and some other references, calculated the luminosity and averaged values for z, $\alpha_{\rm X}^{\rm ph}$, $\alpha_\gamma^{\rm ph}$, $\log \nu L_{\rm R}$, $\log \nu L_{\rm O}$, $\log \nu L_{\rm X}$, $\log \nu L_\gamma$, $\alpha_{\rm RO}$ and $\alpha_{\rm OX}$ for TeV BLs and the subgroups of BLs, and made some comparisons by using the K-S test and correlation analysis. The results are listed in Tables 2−4 and shown in Figures 1–12.

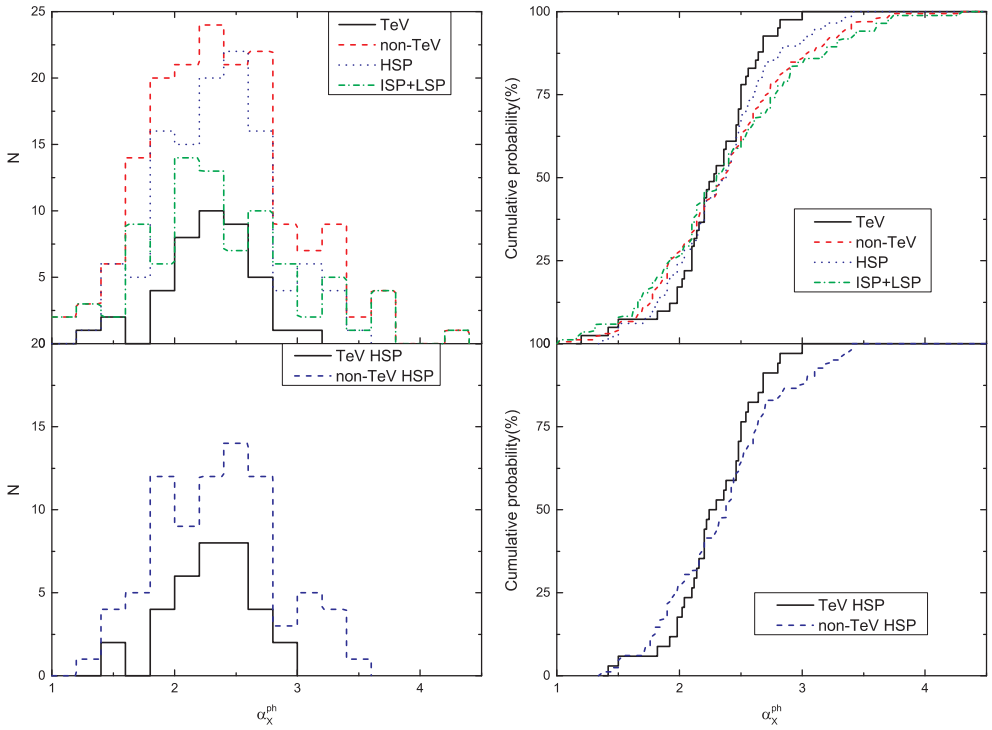

Fig. 2 The distribution of X-ray photon index (*left panels*) and the cumulative probability (*right panels*) for the whole sample (*upper panels*), and for the HSP BL Lacs (*lower panels*). In the upper panels the solid line stands for TeV sources, the dashed line for non-TeV sources, the dotted line for HSP, and the dash-dotted line for ISP+LSP. In the lower panels the solid line stands for TeV HSP BL Lacs and the dashed line for non-TeV HSP BL Lacs.

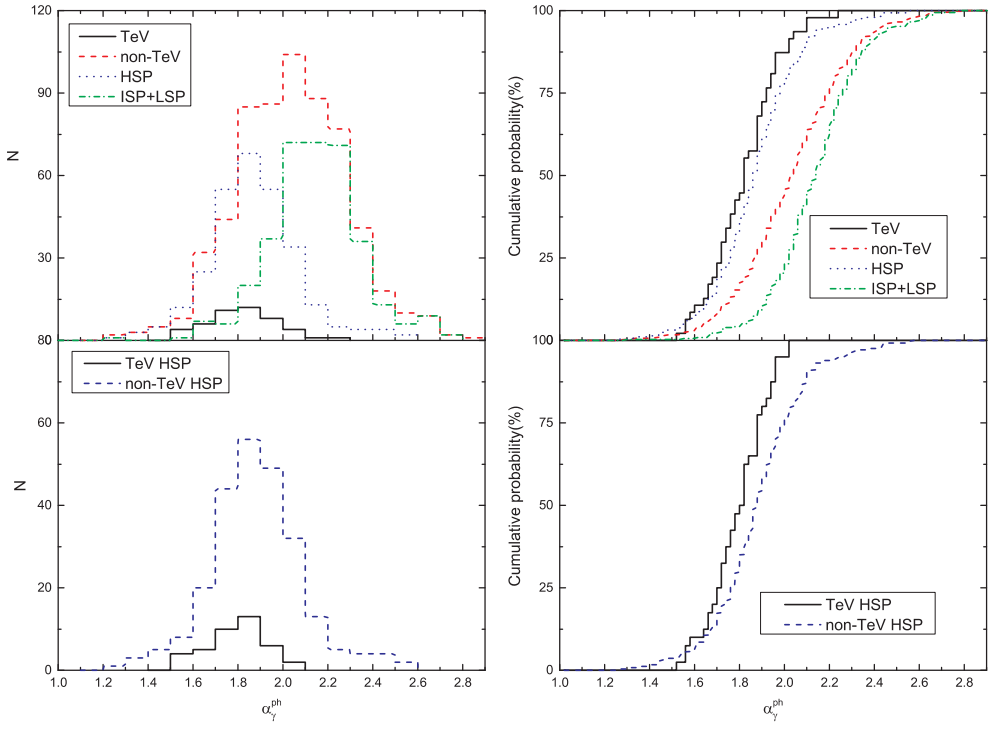

Fig. 3 The distribution of γ-ray photon index (*left panels*) and the cumulative probability (*right panels*) for the whole sample (*upper panels*), and for the HSP BL Lacs (*lower panels*). In the upper panels the solid line stands for TeV sources, the dashed line for non-TeV sources, the dotted line for HSP, and the dash-dotted line for ISP+LSP. In the lower panels the solid line stands for TeV HSP BL Lacs and the dashed line for non-TeV HSP BL Lacs.

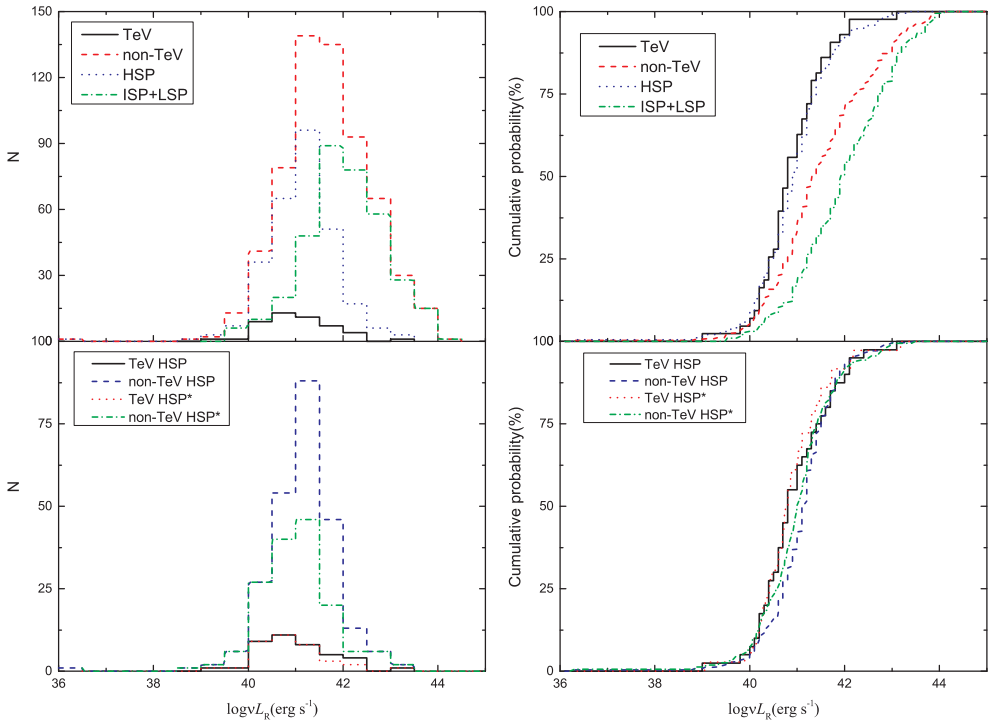

Fig. 4 The distribution of radio luminosity (*left panels*) and the cumulative probability (*right panels*) for the whole sample (*upper panels*) and for the HSP BL Lacs (*lower panels*). In the upper panels the solid line stands for TeV sources, the dashed line for non-TeV sources, the dotted line for HSP, and the dash-dotted line for ISP+LSP. In the lower panels the solid line stands for TeV HSP BL Lacs, the dashed line for non-TeV HSP BL Lacs, the dotted line for TeV HSP BL Lacs with redshift and the dash-dotted line for non-TeV HSP BL Lacs with redshift.

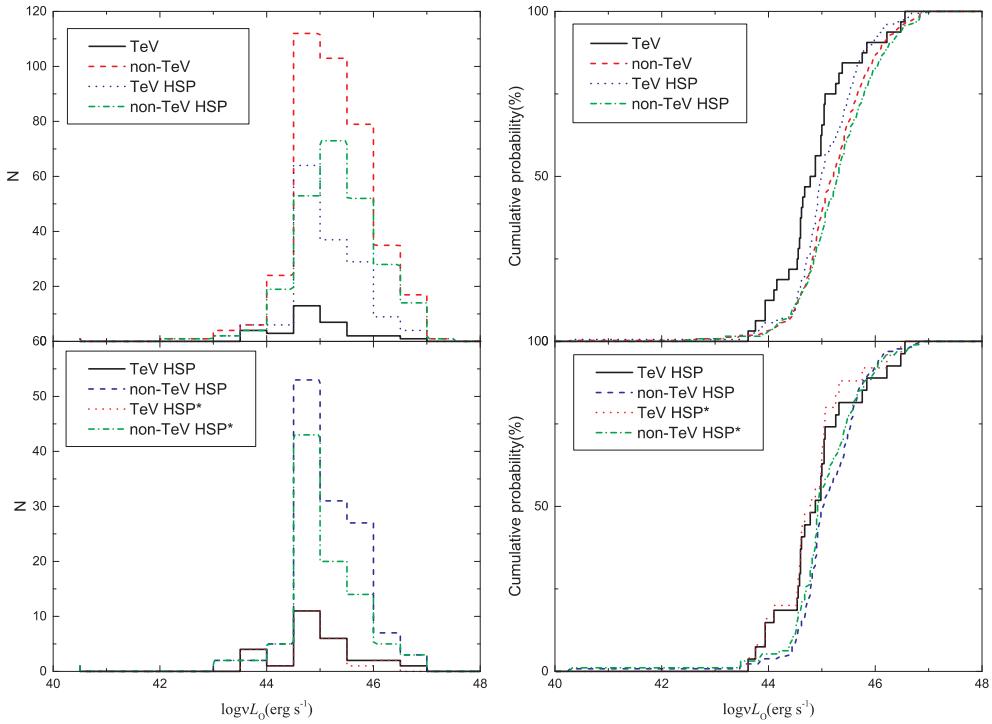

Fig. 5 The distribution of optical luminosity (*left panels*) and the cumulative probability (*right panels*) for the whole sample (*upper panels*), and for the HSP BL Lacs (*lower panels*). In the upper panels the solid line stands for TeV sources, the dashed line for non-TeV sources, the dotted line for HSP, and the dash-dotted line for ISP+LSP. In the lower panels the solid line stands for TeV HSP BL Lacs, the dashed line for non-TeV HSP BL Lacs, the dotted line for TeV HSP BL Lacs with redshift and the dash-dotted line for non-TeV HSP BL Lacs with redshift.

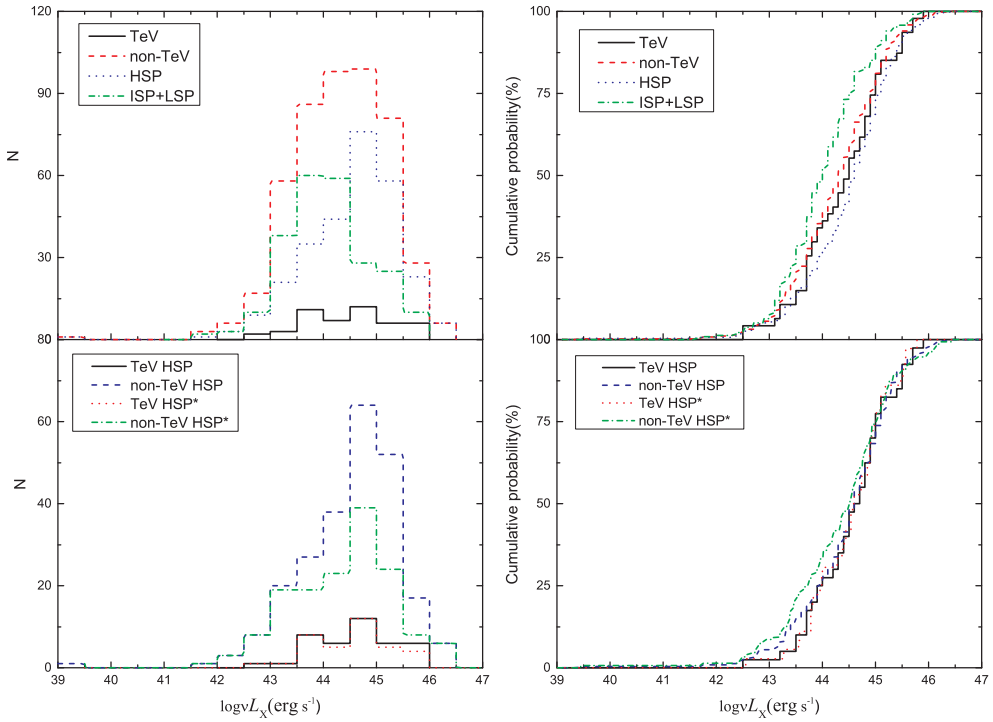

Fig. 6 The distribution of X-ray luminosity (*left panels*) and the cumulative probability (*right panels*) for the whole sample (*upper panels*), and for the HSP BL Lacs (*lower panels*). In the upper panels the solid line stands for TeV sources, the dashed line for non-TeV sources, the dotted line for HSP, and the dash-dotted line for ISP+LSP. In the lower sub-panel the solid line stands for TeV HSP BL Lacs, the dashed line for non-TeV HSP BL Lacs, the dotted line for TeV HSP BL Lacs with redshift and the dash-dotted line for non-TeV HSP BL Lacs with redshift.

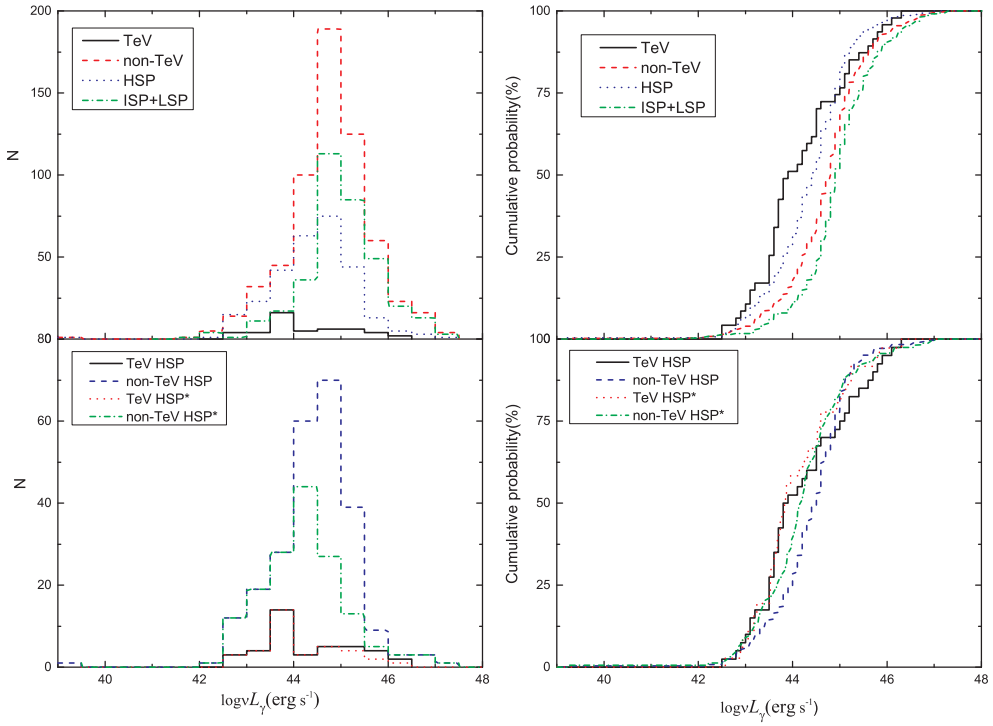

Fig. 7 The distribution of γ-ray luminosity (*left panels*) and the cumulative probability (*right panels*) for the whole sample (*upper panels*), and for the HSP BL Lacs (*lower panels*). In the upper panels the solid line stands for TeV sources, the dashed line for non-TeV sources, the dotted line for HSP, and the dash-dotted line for ISP+LSP. In the lower panels the solid line stands for TeV HSP BL Lacs, the dashed line for non-TeV HSP BL Lacs, the dotted line for TeV HSP BL Lacs with redshift and the dash-dotted line for non-TeV HSP BL Lacs with redshift.

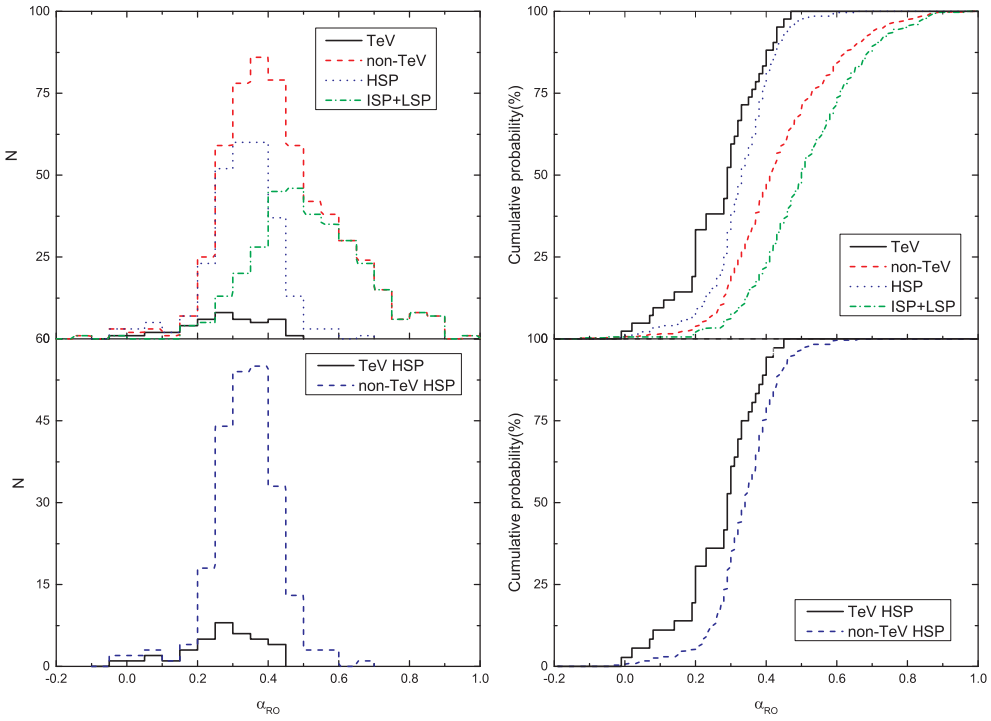

Fig. 8 The distribution of effective spectral index $\alpha_{\rm RO}$ (*left panels*) and the cumulative probability (*right panels*) for the whole sample (*upper panels*), and for the HSP BL Lacs (*lower panels*). In the upper panels the solid line stands for TeV sources, the dashed line for non-TeV sources, the dotted line for HSP, and the dash-dotted line for ISP+LSP. In the lower panels the solid line stands for TeV HSP BL Lacs and the dashed line for non-TeV HSP BL Lacs.

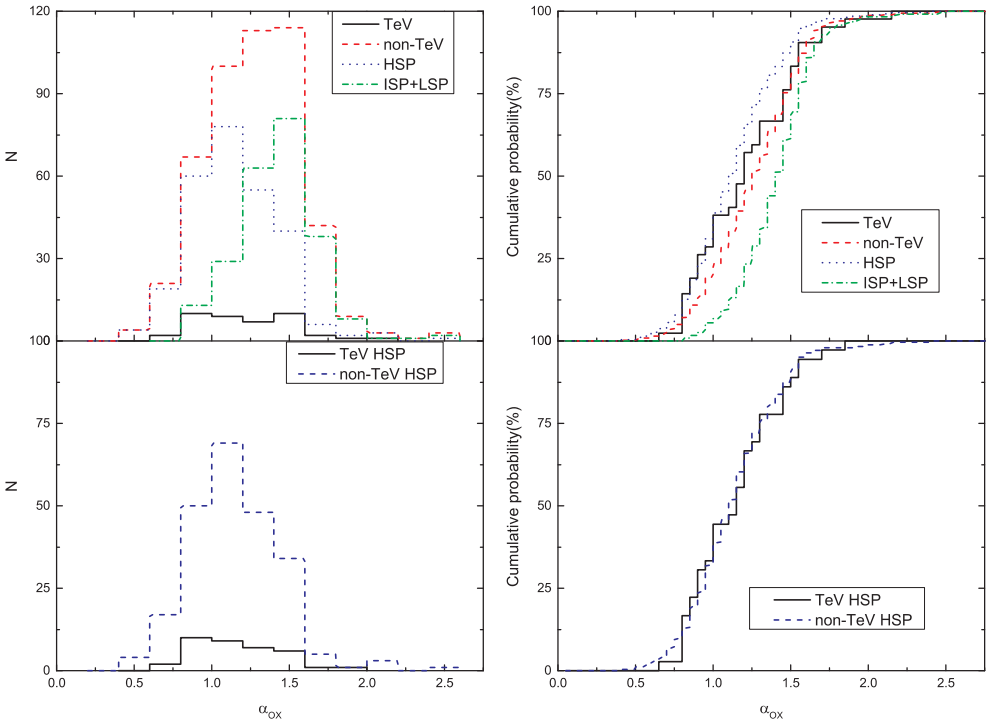

Fig. 9 The distribution of effective spectral index $\alpha_{\rm OX}$ (*left panels*) and the cumulative probability (*right panels*) for the whole sample (*upper panel*), and for the HSP BL Lacs (*lower panel*). In the upper panels the solid line stands for TeV sources, the dashed line for non-TeV sources, the dotted line for HSP, and the dash-dotted line for ISP+LSP. In the lower panels the solid line stands for TeV HSP BL Lacs and the dashed line for non-TeV HSP BL Lacs.

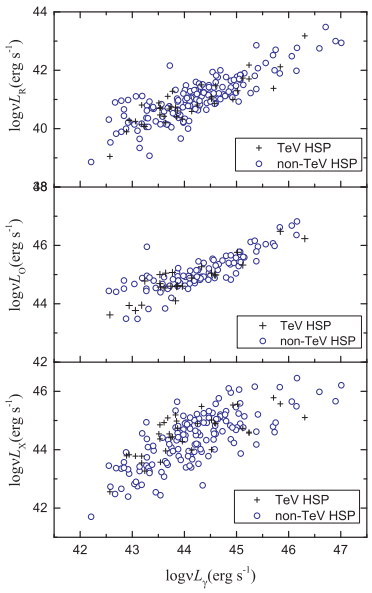

Fig. 10 Plot of the radio (*top*), optical (*middle*), and X-ray (*bottom*) luminosities against the γ-ray luminosity for HSP BL Lacs. In each panel, the plus symbols represent TeV HSP BL Lacs and the circle symbols represent non-TeV HSP BL Lacs.

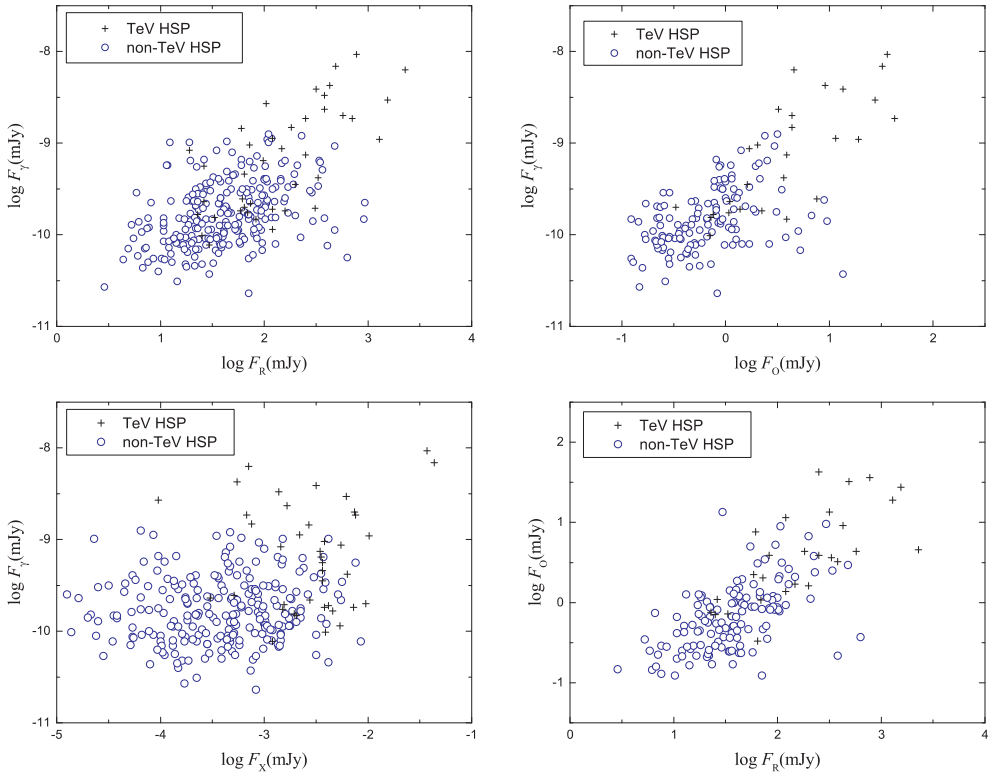

Fig. 11 Plot of the γ-ray flux against the radio flux (*left upper panel*), the optical flux (*right upper panel*) and the X-ray flux (*left lower panel*) for HSP BL Lacs. A plot of the optical flux against the radio flux for HSP BL Lacs is in the right lower panel. In each panel, the plus symbols represent TeV HSP BL Lacs and the circle symbols represent non-TeV HSP BL Lacs.

4.1 Averaged Values

TeV BLs and non-TeV BLs: From Tables 2 and 3 and Figures 1–9, we can see a clear difference between TeV BLs and non-TeV BLs in γ-ray photon spectral index (α_γ) with a probability for the two groups to come from the same distribution being $p < 10^{-8}$, that is $p < 10^{-13}$ in redshift (z), $p < 10^{-4}$ in radio luminosity ($\log \nu L_{\rm R}$) and γ-ray luminosity ($\log \nu L_\gamma$), and $p < 10^{-7}$ in effective radio-optical spectral index ($\alpha_{\rm RO}$). However, there is no clear difference in X-ray photon spectral index ($\alpha_{\rm X}^{\rm ph}$), optical luminosity ($\log \nu L_{\rm O}$), X-ray luminosity ($\log \nu L_{\rm X}$) or

Table 2 Average Values of *Fermi* BL Lacs

		All	TeV	non-TeV	HSP	ISP+LSP	TeV HSP	non-TeV HSP	Figure
(1)	(2)	(3)	(4)	(5)	(6)	(7)	(8)	(9)	(10)
Redshift	Average	0.463 ± 0.418	0.157 ± 0.116	0.500 ± 0.426	0.336 ± 0.322	0.596 ± 0.467	0.170 ± 0.123	0.347 ± 0.341	Fig. 1
	Number	403	43	360	193	197	36	157	
$\alpha_{\rm X}^{\rm ph}$	Average	2.352 ± 0.534	2.273 ± 0.369	2.371 ± 0.567	2.336 ± 0.447	2.337 ± 0.644	2.295 ± 0.350	2.353 ± 0.483	Fig. 2
	Number	206	41	165	116	85	34	82	
$\alpha_{\gamma}^{\rm ph}$	Average	2.023 ± 0.246	1.827 ± 0.156	2.038 ± 0.246	1.875 ± 0.200	2.143 ± 0.206	1.798 ± 0.129	1.888 ± 0.207	Fig. 3
	Number	662	47	615	286	353	40	246	
$\log \nu L_{\rm R}$	Average	41.599 ± 0.912	41.028 ± 0.750	41.643 ± 0.909	41.119 ± 0.753	42.024 ± 0.828	40.993 ± 0.789	41.139 ± 0.746	Fig. 4
	Number	662	47	615	286	353	40	246	
$\log \nu L_{\rm R}^{*}$	Average						40.881 ± 0.743	40.002 ± 0.850	Fig. 4
	Number						36	157	
$\log \nu L_{\rm O}$	Average	45.213 ± 0.735	44.885 ± 0.724	45.240 ± 0.730	45.083 ± 0.725	45.316 ± 0.735	44.922 ± 0.763	45.116 ± 0.715	Fig. 5
	Number	416	32	384	158	248	27	131	
$\log \nu L_{\rm O}^{*}$	Average						44.819 ± 0.686	45.042 ± 0.793	Fig. 5
	Number						25	95	
$\log \nu L_{\rm X}$	Average	44.325 ± 0.865	44.435 ± 0.821	44.314 ± 0.869	44.529 ± 0.876	44.065 ± 0.791	44.602 ± 0.748	44.517 ± 0.897	Fig. 6
	Number	530	47	483	277	235	40	237	
$\log \nu L_{\rm X}^{*}$	Average						44.530 ± 0.725	44.341 ± 0.997	Fig. 6
	Number						36	151	
$\log \nu L_{\gamma}$	Average	44.712 ± 0.906	44.232 ± 0.970	44.749 ± 0.892	44.400 ± 0.881	44.988 ± 0.840	44.262 ± 0.999	44.423 ± 0.860	Fig. 7
	Number	662	47	615	286	353	40	246	
$\log \nu L_{\gamma}^{*}$	Average						44.088 ± 0.891	44.190 ± 0.969	Fig. 7
	Number						36	157	
$\alpha_{\rm RO}$	Average	0.425 ± 0.161	0.275 ± 0.116	0.436 ± 0.159	0.328 ± 0.100	0.511 ± 0.156	0.269 ± 0.111	0.337 ± 0.096	Fig. 8
	Number	616	42	574	272	326	36	236	
$\alpha_{\rm OX}$	Average	1.275 ± 0.309	1.227 ± 0.333	1.280 ± 0.307	1.154 ± 0.293	1.426 ± 0.255	1.156 ± 0.289	1.154 ± 0.295	Fig. 9
	Number	519	42	477	268	236	36	232	

Col. (1) gives parameter, Col. (2) averaged value and number in the sample, Col. (3) all the sample, Col. (4) TeV BLs, Col. (5) non-TeV BLs, Col. (6) HSP BLs, Col. (7) ISP+LSP BLs, Col. (8) TeV HSP BLs, Col. (9) non-TeV HSP BLs, and Col. (10) the corresponding figure number. For luminosities of HSP BLs, the samples with available redshift are marked by "$*$." The luminosities are in the unit of erg s^{-1}.

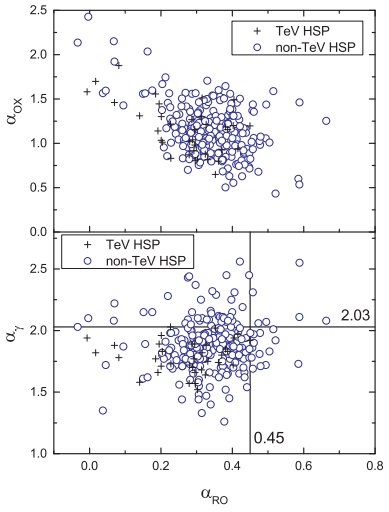

Fig. 12 Plot of the effective spectral index $\alpha_{\rm OX}$ (*upper panel*) and γ-ray photon index (*lower panel*) against the effective spectral index $\alpha_{\rm RO}$ for HSP BL Lacs. In each panel, the circle symbols represent non-TeV HSP BL Lacs and the plus symbols represent TeV HSP BL Lacs.

effective optical-X-ray spectral index ($\alpha_{\rm OX}$) between TeV BLs and non-TeV BLs. The averaged γ-ray photon spectral indexes show that TeV BLs have a harder spectrum than non-TeV BLs. The steeper spectrum of non-TeV BLs makes the TeV emissions be below the sensitivity of TeV detectors so that they cannot be detected. For the known TeV BLs, their redshift is small, and it is possible that the TeV emissions from sources with high redshift may be absorbed by cosmic background emissions. Therefore, it is hard to detect TeV emissions from high redshift. For non-TeV BLs, they are strongly beamed in radio and γ-ray bands, so their radio and γ-ray luminosities are higher than those for TeV BLs. Also, the non-TeV BLs in this work are mainly LBLs and IBLs, which show their synchrotron peak frequencies in the range of infrared to optical bands. Their radio emissions are luminous, which also results in the difference in the effective spectral index $\alpha_{\rm RO}$, with $\alpha_{\rm RO}$ in non-TeV BLs being larger than that in TeV BLs.

TeV BLs and LBLs/IBLs: The difference between TeV BLs and LBLs/IBLs is clear in $\alpha_{\gamma}^{\rm ph}$, z, $\log \nu L_{\rm R}$, $\log \nu L_{\rm O}$, $\log \nu L_{\rm X}$, $\log \nu L_{\gamma}$, $\alpha_{\rm RO}$ and $\alpha_{\rm OX}$, but it is not clear in $\alpha_{\rm X}^{\rm ph}$ ($p = 7.06\%$). For BL Lacs, the X-rays are from synchrotron emissions generated by HBLs whose peak emissions are in the range of UV/X regions, and the summation of synchrotron emissions and inverse Compton emissions generated by LBL/IBL (Fan et al. 2012), which result in there being no clear difference in their X-ray spectral indexes.

TeV BLs and HSP BLs: There is almost no difference between TeV BLs and HSP BLs in $\alpha_{\gamma}^{\rm ph}$, $\alpha_{\rm X}^{\rm ph}$, $\log \nu L_{\rm R}$, $\log \nu L_{\rm O}$, $\log \nu L_{\rm X}$ or $\alpha_{\rm OX}$, but there is a marginal difference in $\log \nu L_{\gamma}$ with a $p = 1.38\%$ and in $\alpha_{\rm RO}$ with a $p = 1.55\%$. Therefore, when we only considered the TeV HSP BLs and non-TeV HSP BLs, we found a clear difference in redshift (z with $p < 10^{-6}$), a marginal difference in γ-ray photon spectral index (α_{γ} with $p = 2.08\%$) and

Table 3 Results of Applying the K-S Test to the Two Samples

Sample	Parameter	N	Average	$d_{\max}$	p
(1)	(2)	(3)	(4)	(5)	(6)
TeV / non-TeV		43 / 360	0.157±0.116 / 0.500±0.426	0.613	$< 10^{-13}$
TeV / HSP	z	43 / 193	0.157±0.116 / 0.336±0.322	0.436	$< 10^{-5}$
TeV / ISP+LSP		43 / 197	0.157±0.116 / 0.596±0.467	0.662	$< 10^{-14}$
TeV HSP / non-TeV HSP		36 / 157	0.170±0.123 / 0.374±0.341	0.502	$< 10^{-6}$
TeV / non-TeV		41 / 165	2.273±0.369 / 2.371±0.567	0.187	14.82%
TeV / HSP	$\alpha_{\rm X}^{\rm ph}$	41 / 116	2.273±0.369 / 2.336±0.447	0.097	87.17%
TeV / ISP+LSP		41 / 85	2.273±0.369 / 2.377±0.644	0.233	7.06%
TeV HSP / non-TeV HSP		34 / 82	2.295±0.350 / 2.353±0.483	0.131	70.56%
TeV / non-TeV		47 / 615	1.827±0.156 / 2.038±0.246	0.471	$< 10^{-8}$
TeV / HSP	$\alpha_{\gamma}^{\rm ph}$	47 / 286	1.827±0.156 / 1.875±0.200	0.137	32.68%
TeV / ISP+LSP		47 / 353	1.827±0.156 / 2.143±0.206	0.691	$< 10^{-19}$
TeV HSP / non-TeV HSP		40 / 246	1.798±0.129 / 1.888±0.207	0.243	2.08%
TeV / non-TeV		47 / 615	41.028±0.750 / 41.643±0.909	0.342	$< 10^{-4}$
TeV / HSP		47 / 286	41.028±0.750 / 41.119±0.753	0.161	20.19%
TeV / ISP+LSP	$\log \nu L_{\rm R}$	47 / 353	41.028±0.750 / 42.024±0.828	0.528	$< 10^{-10}$
TeV HSP / non-TeV HSP		40 / 246	40.993±0.789 / 41.139±0.746	0.233	3.67%
TeV HSP* / non-TeV HSP*		36 / 157	40.881±0.743 / 40.002±0.850	0.191	19.96%
TeV / non-TeV		32 / 384	44.885±0.724 / 45.240±0.730	0.302	0.64%
TeV / HSP		32 / 158	44.885±0.724 / 45.083±0.725	0.247	5.79%
TeV / ISP+LSP	$\log \nu L_{\rm O}$	32 / 248	44.885±0.724 / 45.316±0.735	0.364	0.06%
TeV HSP / non-TeV HSP		27 / 131	44.922±0.763 / 45.116±0.715	0.269	5.85%
TeV HSP* / non-TeV HSP*		25 / 95	44.819±0.686 / 45.042±0.793	0.257	11.00%
TeV / non-TeV		47 / 483	44.435±0.821 / 44.314±0.869	0.106	65.78%
TeV / HSP		47 / 277	44.435±0.821 / 44.529±0.876	0.105	69.09%
TeV / ISP+LSP	$\log \nu L_{\rm X}$	47 / 235	44.435±0.821 / 44.065±0.791	0.260	0.78%
TeV HSP / non-TeV HSP		40 / 237	44.602±0.748 / 44.517±0.897	0.093	87.92%
TeV HSP* / non-TeV HSP*		36 / 151	44.530±0.725 / 44.341±0.997	0.163	36.32%
TeV / non-TeV		47 / 615	44.232±0.970 / 44.749±0.892	0.359	$< 10^{-4}$
TeV / HSP		47 / 286	44.232±0.970 / 44.400±0.881	0.241	1.38%
TeV / HSP($\log \nu_{\rm p}^{\rm s} \geq 16$)	$\log \nu L_{\gamma}$	47 / 121	44.232±0.970 / 44.292±0.681	0.217	6.43%
TeV / ISP+LSP		47 / 353	44.232±0.970 / 44.988±0.840	0.474	$< 10^{-8}$
TeV HSP / non-TeV HSP		40 / 246	44.262±0.999 / 44.423±0.860	0.293	0.37%
TeV HSP* / non-TeV HSP*		36 / 157	44.088±0.891 / 44.190±0.969	0.231	6.97%
TeV / non-TeV		42 / 574	0.275±0.116 / 0.436±0.159	0.455	$< 10^{-7}$
TeV / HSP		42 / 272	0.275±0.116 / 0.328±0.100	0.252	1.55%
TeV / HSP($\log \nu_{\rm p}^{\rm s} \geq 16$)	$\alpha_{\rm RO}$	42 / 115	0.275±0.116 / 0.326±0.093	0.268	1.80%
TeV / ISP+LSP		42 / 326	0.275±0.116 / 0.511±0.156	0.648	$< 10^{-14}$
TeV HSP / non-TeV HSP		36 / 236	0.269±0.111 / 0.337±0.096	0.282	1.06%
TeV / non-TeV		42 / 477	1.227±0.333 / 1.280±0.307	0.152	29.75%
TeV / HSP	$\alpha_{\rm OX}$	42 / 268	1.227±0.333 / 1.154±0.293	0.165	24.07%
TeV / ISP+LSP		42 / 236	1.227±0.333 / 1.426±0.255	0.364	$< 10^{-4}$
TeV HSP / non-TeV HSP		36 / 232	1.156±0.289 / 1.154±0.295	0.081	97.34%

Notes: Col. (1) gives the two tested samples, Col. (2) tested parameter, Col. (3) number in both samples, Col. (4) averaged values and standard deviations, Col. (5) K-S statistic $d_{\max}$, Col. (6) two-tailed significance probability p. The samples with "$*$" are only for the sources with available redshift, and p is the probability for the two distributions to come from the same distribution.

radio to optical spectral index ($\alpha_{\rm RO}$ with $p = 1.06\%$), but no difference in other parameters between TeV HSP BLs and non-TeV HSP BLs. In those different parameters (z, α_{γ}, $\alpha_{\rm RO}$), the averaged values of TeV HSP BLs are lower than those of non-TeV HSP BLs. Does that mean HSP BLs with lower redshift, harder α_{γ} and smaller $\alpha_{\rm RO}$ are good candidates for being TeV emitters? If so, then we can use α_{γ}, $\alpha_{\rm RO}$ and redshift (z) to predict TeV HSP BL Lacs.

From the above analyses, we can clearly see that TeV BL Lacs are different from LBLs/IBLs, but are similar to HSP BL Lacs. If we only take HSP BL Lacs into account, then we find that TeV HSP BL Lacs are quite similar to non-TeV HSP BL Lacs except that there is a difference in redshift and marginal differences in α_{γ} and $\alpha_{\rm RO}$ as shown in the lower panel of Figure 12, which demonstrates $\alpha_{\rm RO} \leq 0.45$ and $\alpha_{\gamma} \leq 2.03$ for TeV HSP BL Lacs.

Taking only TeV and non-TeV HSP BLs into account, we can see that the flux densities for TeV HSP BLs are averagely higher than non-TeV HSP BLs: They are 2.161 ± 0.536 (TeV HSP) vs 1.613 ± 0.458 (non-TeV HSP) for $\log F_{\rm R}$; 0.594 ± 0.581 (TeV HSP) vs -0.174 ± 0.422 (non-TeV HSP) for $\log F_{\rm O}$; -2.564 ± 0.510 (TeV HSP) vs -3.419 ± 0.589 (non-TeV HSP) for $\log F_{\rm X}$; and -9.169 ± 0.578 (TeV HSP) vs -9.768 ± 0.352 (non-TeV HSP) for $\log F_{\gamma}$. The differences can also be seen from Figure 11.

Those differences indicate that TeV HSP BLs tend to have higher fluxes than non-TeV ones. The fluxes of non-TeV HSP BLs may be very low in the TeV band so that they cannot be detected, thus more sensitive telescopes are

Table 4 Correlations of Fermi HSP BL Lacs

y	x	Samples	N	A	B	r	p
(1)	(2)	(3)	(4)	(5)	(6)	(7)	(8)
$\log \nu L_\gamma$	$\log \nu L_{\rm R}$	TeV HSP	36	1.052 ± 0.099	1.087 ± 4.041	0.877	2.31×10^{-12}
		non-TeV HSP	157	0.981 ± 0.047	3.963 ± 1.913	0.861	2.85×10^{-47}
$\log \nu L_\gamma$	$\log \nu L_{\rm O}$	TeV HSP	25	1.152 ± 0.117	-7.611 ± 5.242	0.899	1.02×10^{-9}
		non-TeV HSP	95	1.069 ± 0.059	-3.926 ± 2.659	0.883	2.89×10^{-32}
$\log \nu L_\gamma$	$\log \nu L_{\rm X}$	TeV HSP	36	0.869 ± 0.149	5.375 ± 6.633	0.707	1.40×10^{-6}
		non-TeV HSP	151	0.756 ± 0.048	10.638 ± 2.143	0.788	2.95×10^{-33}
$\log F_\gamma$	$\log F_{\rm R}$	TeV HSP	40	0.752 ± 0.126	-10.794 ± 0.280	0.696	6.00×10^{-7}
		non-TeV HSP	246	0.299 ± 0.045	-10.250 ± 0.076	0.389	2.66×10^{-10}
$\log F_\gamma$	$\log F_{\rm O}$	TeV HSP	27	0.798 ± 0.113	-9.590 ± 0.109	0.769	2.76×10^{-6}
		non-TeV HSP	131	0.318 ± 0.066	-9.780 ± 0.030	0.392	3.73×10^{-6}
$\log F_\gamma$	$\log F_{\rm X}$	TeV HSP	40	0.073 ± 0.184	-8.982 ± 0.480	0.064	69.3%
		non-TeV HSP	237	0.054 ± 0.039	-9.585 ± 0.136	0.089	17.4%
$\log F_{\rm O}$	$\log F_{\rm R}$	TeV HSP	27	0.744 ± 0.147	-1.076 ± 0.340	0.711	3.19×10^{-5}
		non-TeV HSP	131	0.557 ± 0.071	-1.047 ± 0.116	0.567	1.58×10^{-12}

Notes: Col. (1) gives dependent parameter, Col. (2) independent parameter, Col. (3) sample, Col. (4) number of data points in the sample, Col. (5) slope, Col. (6) intercept, Col. (7) correlation coefficient, and Col. (8) chance probability.

required. As we noted, BL Lacs have rapid and large variations, so the TeV emissions are likely to cycle. Therefore, some TeV sources cannot be detected in the TeV band sometimes, and a long term TeV monitoring program could detect more BL Lacs. In addition, the difference in fluxes between TeV HSP BLs and non-TeV HSP BLs could be another criterion to predict TeV emitter candidates.

4.2 Correlations

From luminosity-luminosity correlation analysis of TeV HSP BL Lacs, we can see that there is a close correlation between γ-ray luminosity and the lower energetic bands. Those correlation coefficients and chance probabilities are: $r = 0.877$ and $p = 2.31 \times 10^{-12}$ for $\log \nu L_\gamma$ vs $\log \nu L_{\rm R}$, $r = 0.899$ and $p = 1.02 \times 10^{-9}$ for $\log \nu L_\gamma$ vs $\log \nu L_{\rm O}$, and $r = 0.707$ and $p = 1.40 \times 10^{-6}$ for $\log \nu L_\gamma$ vs $\log \nu L_{\rm X}$, see Table 4 and Figure 10. We also found that the slopes of correlations for TeV HSP BLs are similar to those for non-TeV HSP BLs, and the $\log \nu L_\gamma$ vs $\log \nu L_{\rm R}$ correlation is strongest. The strong γ-ray vs radio correlation was also discussed by other authors (Dondi & Ghisellini 1995; Muecke et al. 1997; Xie et al. 1997; Zhou et al. 1997; Fan et al. 1998, 2012, 2015, 2016, submitted; Cheng et al. 2000; Yang & Fan 2005; Giroletti et al. 2010, 2012; Pushkarev et al. 2010; Linford et al. 2011; Yang et al. 2012b,a, 2014; Li et al. 2015).

For luminosity-luminosity correlation, it is known that all luminosities are correlated with redshift (z), therefore luminosity-luminosity correlation may be caused by the redshift effect (Kendall & Stuart 1979). In this case, one should remove the redshift effect. To do so, we used the method introduced by Padovani (1992) as in our previous work (Fan et al. 2013b, 2015). If variables i and j are correlated with a third one k, then the correlation between i and j should exclude the k effect. In this sense, for three variables i, j and k, if the correlation coefficients of the relation between any two variables of them are expressed as r_{ij}, r_{ik} and r_{jk} respectively, then for the correlation coefficient r_{ij} to be excluded, the k effect is expressed as $r_{ij,k} = (r_{ij} - r_{ik}r_{jk})/\sqrt{(1-r_{ik}^2)(1-r_{jk}^2)}$. When the method is applied to the correlations between any two luminosities, the correlation coefficients after removing the redshift effect are: For $\log \nu L_\gamma$ vs $\log \nu L_{\rm R}$, $r_{\gamma R,z}$ = 0.743 with a chance probability $p_{\gamma R,z} = 7.17 \times 10^{-7}$ for TeV HSP BLs, and $r_{\gamma R,z}$ = 0.400 with $p_{\gamma R,z} = 4.52 \times 10^{-7}$ for non-TeV HSP BLs. For $\log \nu L_\gamma$ vs $\log \nu L_{\rm O}$, $r_{\gamma O,z}$ = 0.811 with $p_{\gamma O,z} = 3.52 \times 10^{-6}$ for TeV HSP BLs, and $r_{\gamma O,z}$ = 0.375 with $p_{\gamma O,z} = 3.0 \times 10^{-4}$ for non-TeV HSP BLs; and for $\log \nu L_\gamma$ vs $\log \nu L_{\rm X}$, $r_{\gamma X,z}$ = 0.255 with $p_{\gamma X,z} = 9.3\%$ for TeV HSP BLs, and $r_{\gamma X,z}$ = 0.085 with $p_{\gamma X,z} = 15.91\%$ for non-TeV HSP BLs. It is clear that after removing the redshift effect, there are still correlations for $\log \nu L_\gamma$ vs $\log \nu L_{\rm R}$ and for $\log \nu L_\gamma$ vs $\log \nu L_{\rm O}$ for TeV HSP BL Lacs, but there is no correlation for $\log \nu L_\gamma$ vs $\log \nu L_{\rm X}$. The results are consistent with those for flux-flux correlation analysis: namely $r = 0.696$ with $p = 6.00 \times 10^{-7}$ for $\log F_\gamma$ vs $\log F_{\rm R}$, $r = 0.769$ with $p = 2.76 \times 10^{-6}$ for $\log F_\gamma$ vs $\log F_{\rm O}$, and $r = 0.064$ with $p = 69.3\%$ for $\log F_\gamma$ vs $\log F_{\rm X}$. For the non-TeV HSP BLs, results show that the correlation coefficients are less than those in TeV HSP after removing the redshift effect, and all the correlation coefficients are less than 0.4, which is very different from the correlation before removing the redshift effect. The results are also consistent with those for flux-flux correlation analysis: $r = 0.389$ with $p = 2.66 \times 10^{-10}$ for $\log F_\gamma$ vs $\log F_{\rm R}$, $r = 0.392$ with $p = 3.73 \times 10^{-6}$ for $\log F_\gamma$ vs $\log F_{\rm O}$, and $r = 0.089$ with $p = 17.4\%$ for $\log F_\gamma$ vs $\log F_{\rm X}$.

For flux-flux correlations, both TeV HSP BLs and non-TeV HSP BLs show strong correlations in $\log F_\gamma$ vs $\log F_{\rm R}$, $\log F_\gamma$ vs $\log F_{\rm O}$, and $\log F_{\rm O}$ vs $\log F_{\rm R}$ with chance probabilities being $p < 10^{-4}$. In those flux-flux correlations, the slopes of TeV HSP BLs are steeper than those of non-TeV HSP BLs, but the corresponding intercepts are very close, which suggest that TeV HSP BLs tend to have higher energy photons (Fig. 11). However, for both

TeV and non-TeV HSP BLs, no correlation was found between $\log F_\gamma$ and $\log F_{\rm X}$.

Dondi & Ghisellini (1995) found correlations between γ-ray luminosity and lower energy bands (including the radio, optical and X-ray bands) of blazars, and the γ-ray vs radio band correlation still exists even after removing the redshift effect. However, they did not discuss the correlations of γ-ray vs optical or γ-ray vs X-ray since they thought that optical and X-ray emissions were contaminated by other emissions. Our results are consistent with theirs. The correlation between X-ray and γ-ray emissions are obtained by some surveys in a long period of observations or some samples of blazars (Li et al. 2013; Bi et al. 2014; Fraija et al. 2015). For example, Fraija et al. (2015) found a strong correlation between the GeV γ-rays and the optical/hard-X ray emissions for Mrk 421 associated with the flare in 2013. However, no correlation was found between γ-ray and the X-ray band for PKS 1510-089 during its high activity period from 2008 to 2009 (Abdo et al. 2010a). From our analysis, there is no correlation between γ-ray and X-ray flux, suggesting that the γ-ray and X-ray emissions are composed of different emission components even though the X-ray emissions in HSP BL Lac are from the synchrotron self-Compton (SSC) process (Fan et al. 2012).

For spectral index correlation, we can see that there is an anti-correlation between $\alpha_{\rm OX}$ and $\alpha_{\rm RO}$ for TeV HSP BL Lacs and non-TeV HSP BL Lacs: $\alpha_{\rm OX}$ = $-(1.445 \pm 0.373)\alpha_{\rm RO}$ + (1.545 $\pm$ 0.108) for 36 TeV HSP BL Lacs with a correlation coefficient $r = -0.554$ and a chance probability $p = 4.59 \times 10^{-4}$, and $\alpha_{\rm OX}$ = $-$(1.422 $\pm$ 0.180) $\alpha_{\rm RO}$ + (1.634 $\pm$ 0.063) for 232 non-TeV HSP BL Lacs with a correlation coefficient $r = -0.462$ and a chance probability $p = 1.10 \times 10^{-13}$. The corresponding plots are shown in the upper panel of Figure 12.

4.3 Mechanism

γ-ray emissions are still an interesting topic for blazars, and the *Fermi* mission has provided us with a good opportunity to re-visit the γ-ray mechanism by detecting a lot of blazars (Abdo et al. 2010b, Nolan et al. 2012, Acero et al. 2015; Ackermann et al. 2015). As we discussed in our previous work (Fan et al. 2013a, 2014), the γ-ray emissions are mainly due to soft photons upscattered by Inverse Compton onto relativistic electrons, or to synchrotron emission/pion decay of secondary particles produced in a proton-induced cascade (Mannheim & Biermann 1992; Mannheim 1993; Cheng & Ding 1994). For LBLs, they have low peak synchrotron emissions with $\log \nu_p < 14.0$ Hz and their inverse Compton emissions peak at $\log \nu_{IC} < 1$ GeV while for HBLs, they have a synchrotron peak frequency of $\log \nu_p > 15$ Hz and their inverse Compton emissions peak at $\log \nu_{IC} > 100$ GeV (Abdo et al. 2009). Therefore, the emissions in the 1$\sim$100 GeV region correspond to the inverse-Compton emission tail, which have a soft spectrum for LBLs, and the emissions in the 1$\sim$100 GeV region correspond to the inverse-Compton emissions before reaching the peak emissions and have a flat spectrum for HBLs. That is why TeV HSP BLs have a flat spectrum (Fan et al. 2012). In this sense, we think that SSC will be responsible for γ-ray emissions for HBLs and particularly for TeV HSP BLs. Fortunately, the SEDs of some blazars can be fitted by a one-zone SSC model in some surveys (Sambruna et al. 2000; Albert et al. 2007; Aleksić et al. 2015a). Aleksić et al. (2015b) found that the SSC model gives a satisfactory description of the observed multi-wavelength spectral energy distribution for PG 1553+113 during the flare. Zhang et al. (2012) compiled the broadband SED data for 24 TeV BL Lac objects and found that these SEDs can be explained well with the SSC model. Abdo et al. (2014) believed the TeV emissions from Mrk 421 are produced by leptonic SSC emissions. After three years of observations of Mrk 421, they found that the TeV activity, measured in what is called duty cycle, which is consistent with the X-ray activity and therefore favors the SSC emission mechanism. If we use the SSC model to explain the TeV radiation, the HSP BL Lacs, which have high-synchrotron-peaked frequency, will have more probability to produce TeV radiation. Our results of γ-ray and radio correlations obtained by luminosity-luminosity and flux-flux relationships also support an SSC process for γ-rays.

4.4 Conclusions

In this work, we compiled the radio, optical, X-ray and γ-ray data for a sample of 662 *Fermi* BL Lacs (47 are TeV BL Lacs and 615 are non-TeV BL Lacs) from 3LAC (Ackermann et al. 2015) and other references, calculated the flux density and luminosity, compared the averaged values and investigated luminosity-luminosity and flux-flux correlations for TeV BL Lacs and subclasses of BL Lacs. We have drawn the following conclusions:

(1) TeV BL Lacs are different from LBLs and IBLs in the distributions of $\alpha_\gamma^{\rm ph}$, z, $\log \nu L_{\rm R}$, $\log \nu L_{\rm O}$, $\log \nu L_{\rm X}$, $\log \nu L_\gamma$, $\alpha_{\rm RO}$ and $\alpha_{\rm OX}$, but not in that of $\alpha_{\rm X}^{\rm ph}$. TeV BL Lacs tend to show similar properties as HSP BL Lacs in $\alpha_\gamma^{\rm ph}$, $\alpha_{\rm X}^{\rm ph}$, $\log \nu L_{\rm R}$, $\log \nu L_{\rm O}$, $\log \nu L_{\rm X}$ and $\alpha_{\rm OX}$, but not in $\log \nu L_\gamma$ or $\alpha_{\rm RO}$;
(2) TeV HSP BL Lacs show different distributions of redshift from non-TeV HSP BL Lacs, marginally different distributions in $\alpha_{\rm RO}$ and α_γ, but no difference in other parameters. So, HSP BL Lacs with low redshift, low $\alpha_{\rm RO}$ and α_γ, but high fluxes are good TeV emitter candidates;
(3) There is a significant correlation between γ-ray and radio bands and between γ-ray and optical bands, but there is no correlation between γ-ray and X-ray bands for TeV HSP BLs;
(4) The γ-ray emissions in HSP BLs are from the SSC model.

Acknowledgements This work is partially supported by the National Natural Science Foundation of China (Grant

Nos. 10633010, 11173009, U1431112 and U1531245), the Innovation Foundation of Guangzhou University (IFGZ), Guangdong Province Universities and Colleges Pearl River Scholar Funded Scheme (GDUPS, 2009), Yangcheng Scholar Funded Scheme (10A027S), and support for Astrophysics Key Subjects of Guangdong Province and Guangzhou City. We thank the referee for the comments and suggestions which improved the manuscript.

References

Abdo, A. A., Ackermann, M., Ajello, M., et al. 2009, ApJ, 700, 597
Abdo, A. A., Ackermann, M., Agudo, I., et al. 2010a, ApJ, 721, 1425
Abdo, A. A., Ackermann, M., Ajello, M., et al. 2010b, ApJS, 188, 405
Abdo, A. A., Ackermann, M., Agudo, I., et al. 2010c, ApJ, 716, 30
Abdo, A. A., Abeysekara, A. U., Allen, B. T., et al. 2014, ApJ, 782, 110
Acero, F., Ackermann, M., Ajello, M., et al. 2015, ApJS, 218, 23
Ackermann, M., Ajello, M., Atwood, W. B., et al. 2015, ApJ, 810, 14
Ajello, M., Costamante, L., Sambruna, R. M., et al. 2009, ApJ, 699, 603
Albert, J., Aliu, E., Anderhub, H., et al. 2007, ApJ, 663, 125
Aleksić, J., Ansoldi, S., Antonelli, L. A., et al. 2015a, A&A, 573, A50
Aleksić, J., Ansoldi, S., Antonelli, L. A., et al. 2015b, MNRAS, 450, 4399
Bastieri, D., Ciprini, S., & Gasparrini, D. 2011, Journal of Astrophysics and Astronomy, 32, 169
Bi, X., He, W., Tian, J., Ding, Z., & Ge, S. 2014, Journal of Astrophysics and Astronomy, 35, 329
Brinkmann, W., Yuan, W., & Siebert, J. 1997a, A&A, 319, 413
Brinkmann, W., Siebert, J., Feigelson, E. D., et al. 1997b, A&A, 323, 739
Brinkmann, W., Laurent-Muehleisen, S. A., Voges, W., et al. 2000, A&A, 356, 445
Cheng, K. S., & Ding, W. K. Y. 1994, A&A, 288, 97
Cheng, K. S., Zhang, X., & Zhang, L. 2000, ApJ, 537, 80
Donato, D., Sambruna, R. M., & Gliozzi, M. 2005, A&A, 433, 1163
Dondi, L., & Ghisellini, G. 1995, MNRAS, 273, 583
Fan, J. H., Adam, G., Xie, G. Z., et al. 1998, A&A, 338, 27
Fan, J. H., Yang, J. H., Yuan, Y. H., et al. 2012, ApJ, 761, 125
Fan, J.-H., Yang, J.-H., Liu, Y., & Zhang, J.-Y. 2013a, RAA (Research in Astronomy and Astrophysics), 13, 259
Fan, J., Yang, J. H., Zhang, J.-Y., et al. 2013b, PASJ, 65, 25
Fan, J.-H., Bastieri, D., Yang, J.-H., et al. 2014, RAA (Research in Astronomy and Astrophysics), 14, 1135
Fan, J. H., Yang, J. H., Liu, Y., et al. 2015, International Journal of Modern Physics A, 30, 1545020
Fraija, N., Cabrera, J. I., Benítez, E., & Hiriart, D. 2015, arXiv:1508.01438
Giroletti, M., Reimer, A., Fuhrmann, L., & Pavlidou, V. 2010, in Astronomical Society of the Pacific Conference Series, 427, Accretion and Ejection in AGN: a Global View, eds. L. Maraschi, G. Ghisellini, R. Della Ceca, & F. Tavecchio, 283
Giroletti, M., Pavlidou, V., Reimer, A., et al. 2012, Advances in Space Research, 49, 1320
Green, P. J., Aldcroft, T. L., Richards, G. T., et al. 2009, ApJ, 690, 644
Gupta, A. C., Deng, W. G., Joshi, U. C., et al. 2008, New Astron., 13, 375
Kapanadze, B. Z. 2013, AJ, 145, 31
Kendall, M., & Stuart, A. 1979, The Advanced Theory of Statistics, 2, Inference and Relationship (London: Griffin, 1979, 4th ed.)
Lamer, G., Brunner, H., & Staubert, R. 1996, A&A, 311, 384
Laurent-Muehleisen, S. A., Kollgaard, R. I., Feigelson, E. D., et al. 1999, ApJ, 525, 127
Li, B., Zhang, H., Zhang, X., et al. 2013, Ap&SS, 347, 349
Li, H.-Z., Chen, L.-E., Jiang, Y.-G., & Yi, T.-F. 2015, RAA (Research in Astronomy and Astrophysics), 15, 929
Linford, J. D., Taylor, G. B., Romani, R. W., et al. 2011, ApJ, 726, 16
Lott, B., Cavazzuti, E., Ciprini, S., Cutini, S., & Gasparrini, D. 2015, in IAU Symposium, 313, Extragalactic Jets from Every Angle, eds. F. Massaro, C. C. Cheung, E. Lopez, & A. Siemiginowska, 12
Mannheim, K. 1993, Phys. Rev. D, 48, 2408
Mannheim, K., & Biermann, P. L. 1992, A&A, 253, L21
Massaro, E., Maselli, A., Leto, C., et al. 2015, Ap&SS, 357, 75
Muecke, A., Pohl, M., Reich, P., et al. 1997, A&A, 320, 33
Nolan, P. L., Abdo, A. A., Ackermann, M., et al. 2012, ApJS, 199, 31
Padovani, P. 1992, A&A, 256, 399
Pushkarev, A. B., Kovalev, Y. Y., & Lister, M. L. 2010, ApJ, 722, L7
Reich, W., Fürst, E., Reich, P., et al. 2000, A&A, 363, 141
Romero, G. E., Cellone, S. A., Combi, J. A., et al. 2002, A&A, 390, 431
Sambruna, R. M., Aharonian, F. A., Krawczynski, H., et al. 2000, ApJ, 538, 127
Wills, B. J., Wills, D., Breger, M., et al. 1992, ApJ, 398, 454
Wright, E. L. 2006, PASP, 118, 1711
Xie, G. Z., Zhang, Y. H., & Fan, J. H. 1997, ApJ, 477, 114
Yang, J.-H., & Fan, J.-H. 2005, ChJAA (Chin. J. Astron. Astrophys.), 5, 229
Yang, J., Fan, J., Nie, J., & Yang, R. 2012a, Science China Physics, Mechanics, and Astronomy, 55, 2179
Yang, J., Fan, J., & Yuan, Y. 2012b, Science China Physics, Mechanics, and Astronomy, 55, 1510
Yang, J. H., Fan, J. H., Hua, T. X., et al. 2014, Ap&SS, 352, 819
Zhang, J., Liang, E.-W., Zhang, S.-N., et al. 2012, ApJ, 752, 157
Zhang, Y.-W., & Fan, J.-H. 2008, ChJAA (Chin. J. Astron. Astrophys.), 8, 385
Zhou, Y. Y., Lu, Y. J., Wang, T. G., et al. 1997, ApJ, 484, L47